



# HHS Public Access

Author manuscript

*Nat Chem Biol.* Author manuscript; available in PMC 2013 June 01.

Published in final edited form as:

*Nat Chem Biol.* 2012 December ; 8(12): 982–989. doi:10.1038/nchembio.1094.

## Divergent allosteric control of the IRE1 $\alpha$ endoribonuclease using kinase inhibitors

Likun Wang<sup>1,2,3,4,10</sup>, B. Gayani K. Perera<sup>6,10</sup>, Sanjay B. Hari<sup>6</sup>, Barun Bhatarai<sup>8</sup>, Bradley J. Backes<sup>1,2</sup>, Markus A. Seeliger<sup>7</sup>, Stephan C. Schürer<sup>8,9</sup>, Scott A. Oakes<sup>5</sup>, Feroz R. Papa<sup>1,2,3,4,10,\*</sup>, and Dustin J. Maly<sup>6,10,\*</sup>

<sup>1</sup>Department of Medicine, University of California, San Francisco. San Francisco, CA 94143. U.S.A.

<sup>2</sup>Lung Biology Center, University of California, San Francisco. San Francisco, CA 94143. U.S.A.

<sup>3</sup>Diabetes Center, University of California, San Francisco. San Francisco, CA 94143. U.S.A.

<sup>4</sup>California Institute for Quantitative Biosciences, University of California, San Francisco. San Francisco, CA 94143. U.S.A.

<sup>5</sup>Department of Pathology, University of California, San Francisco. San Francisco, CA 94143. U.S.A.

<sup>6</sup>Department of Chemistry, University of Washington. Seattle, WA 98195. U.S.A.

<sup>7</sup>Department of Pharmacological Sciences, Stony Brook University Medical School. Stony Brook, NY 11794. U.S.A.

<sup>8</sup>Center for Computational Science, Miller School of Medicine, University of Miami, FL, 33136, USA

<sup>9</sup>Department of Molecular and Cellular Pharmacology, Miller School of Medicine, University of Miami, FL, 33136, USA

### Abstract

Under endoplasmic reticulum (ER) stress, unfolded proteins accumulate in the ER to activate the ER transmembrane kinase/endoribonuclease (RNase)—IRE1 $\alpha$ . IRE1 $\alpha$  oligomerizes, autophosphorylates, and initiates splicing of XBP1 mRNA, thus triggering the unfolded protein response (UPR). Here we show that IRE1 $\alpha$ 's kinase-controlled RNase can be regulated in two

Users may view, print, copy, download and text and data-mine the content in such documents, for the purposes of academic research, subject always to the full Conditions of use: [http://www.nature.com/authors/editorial\\_policies/license.html#terms](http://www.nature.com/authors/editorial_policies/license.html#terms)

\*Correspondence: frpapa@medicine.ucsf.edu (Tel: 415-476-2117/ FAX: 415-514-9656), maly@chem.washington.edu (Tel: 206-543-1653/ FAX: 206-685-7002).

<sup>10</sup>These authors contributed equally to this work

### Author Contributions

F. R. P. and D. J. M. conceived the idea and designed the study. With the guidance of F. R. P. and D. J. M., L. W. designed and performed the biochemical and cellular studies. B. G. K. P. designed and performed all of the chemical syntheses. S. B. H. performed footprinting experiments. B. B. and S. C. S. performed molecular modeling studies. All authors designed experiments, analyzed data, and commented on the manuscript. F. R. P. and D. J. M. co-wrote the paper.

### Competing financial interests

The authors declare no competing financial interests.

distinct modes with kinase inhibitors: one class of ligands occupy IRE1 $\alpha$ 's kinase ATP-binding site to activate RNase-mediated XBP1 mRNA splicing even without upstream ER stress, while a second class can inhibit the RNase through the same ATP-binding site, even under ER stress. Thus, alternative kinase conformations stabilized by distinct classes of ATP-competitive inhibitors can cause allosteric switching of IRE1 $\alpha$ 's RNase—either on or off. As dysregulation of the UPR has been implicated in a variety of cell degenerative and neoplastic disorders, small molecule control over IRE1 $\alpha$  should advance efforts to understand the UPR's role in pathophysiology and to develop drugs for ER stress-related diseases.

---

The UPR is an evolutionarily conserved intracellular signaling pathway triggered when unfolded proteins accumulate in the ER<sup>1,2</sup>. The UPR is believed to be centrally involved in the pathogenesis of numerous cell degenerative disorders, such as diabetes<sup>3</sup> and neurodegeneration, and conversely the inappropriate survival of secretory cell tumors, such as multiple myeloma<sup>4</sup>. Because the UPR normally relegates irremediably ER stressed cells to apoptosis, the ability to control the UPR's cell fate outcomes in both positive and negative directions may provide new therapeutic options for these diseases<sup>5</sup>. To this end, we have been developing pharmacological tools to both activate and inhibit the master regulator of the UPR, a bifunctional enzyme called IRE1 $\alpha$ <sup>6-9</sup>.

IRE1 $\alpha$  is an ER transmembrane protein that becomes activated when unfolded proteins accumulate within the organelle. Through an N-terminal ER luminal domain that senses unfolded proteins, IRE1 $\alpha$  monomers dimerize and potentially oligomerize in the plane of the ER membrane<sup>10-12</sup>. This event juxtaposes cytosolic kinase domains across individual IRE1 $\alpha$  monomers, causing *trans*-autophosphorylation. In turn, autophosphorylation activates the C-terminal RNase domain to catalyze site-specific cleavage of the mRNA encoding the XBP1 transcription factor, excising a 26 nucleotide intervening region<sup>13,14</sup>. Religation of cleaved XBP1 mRNA and translation in the shifted open-reading frame produces the XBP1s (s = spliced) transcription factor, whose gene targets allow the ER to adapt to protein-folding stress.

Genetic analysis shows that activation of IRE1 $\alpha$ 's RNase is normally dependent on kinase autophosphorylation<sup>6</sup>, but we previously identified an unusual relationship between these two domains that allows specific ligands of the kinase domain to bypass the autophosphorylation requirement and trigger RNase activation through ligand occupancy alone<sup>15</sup>. For instance, the orthogonal ATP-competitive inhibitor 1NM-PP1 rescues RNase activity of IRE1 $\alpha$  mutants that lack kinase activity<sup>7,8,15</sup>. Other ligands that interact with the ATP-binding site of wild-type (WT) IRE1 $\alpha$  also activate the RNase directly. For example, the ATP-competitive inhibitor APY29 and the clinically-approved drug sunitinib activate the RNase of yeast<sup>16</sup> and murine IRE1 $\alpha$ <sup>7</sup>.

Given the ability to allosterically activate IRE1 $\alpha$ 's RNase through its kinase domain, we hypothesized that it may be feasible to also inhibit the RNase through the same kinase domain, but with a different class of kinase inhibitors. Two classes of kinase inhibitors—called types I and II—have been identified, which stabilize alternate kinase active site conformations in numerous protein kinase targets<sup>17</sup>. Here we show that a known type I kinase inhibitor and a novel type II kinase inhibitor both shut down IRE1 $\alpha$  *trans*-

autophosphorylation, but have divergent effects on its RNase to activate or inactivate catalytic activity, respectively. Our findings demonstrate that IRE1 $\alpha$  RNase activity can be either up or downregulated through selective targeting of its kinase domain to control UPR signaling, and predict that it may be possible to pharmacologically modulate other kinase-coupled enzymes in a similar way.

## Results

### Divergent modulation of the IRE1 $\alpha$ 's RNase activity

A co-crystal structure of yeast IRE1 bound with APY29—a predicted type I kinase inhibitor—shows that the kinase catalytic domain is in an active conformation, which is a conformation typically adopted by protein kinases when bound to ATP and other type I inhibitors (Fig. 1a)<sup>16,18</sup>. Moreover, two additional co-crystal structures of yeast IRE1 and human IRE1 $\alpha$  bound with ADP show that the kinase domain is similarly in an active conformation<sup>18–20</sup>. By stabilizing IRE1 $\alpha$ 's kinase in the active conformation, these type I inhibitors act as ligands that allosterically activate its adjacent RNase domain. Therefore, we postulated that it might be possible to stabilize IRE1 $\alpha$ 's kinase domain in an alternative conformation, and in so doing disable its RNase activity. To test this notion, we employed a class of small-molecule kinase inhibitors that have been described to selectively stabilize the inactive conformation of the ATP-binding site (type II inhibitors) for a variety of kinases; examples include the clinically-approved drugs imatinib and sorafenib<sup>17,21,22</sup>. The inactive ATP-binding site conformation stabilized by type II inhibitors is characterized by outward movement of the catalytically-important Asp-Phe-Gly (DFG) motif, and is therefore called the DFG-out conformation (Fig. 1a)<sup>17,23</sup>. In contrast, in all three co-crystal structures of IRE1 mentioned previously, the kinase domain adopts the DFG-in conformation<sup>16,19,20</sup>.

Therefore, we hypothesized that stabilizing an inactive ATP-binding site conformation of IRE1 $\alpha$  with type II inhibitors may have inhibitory rather than activating allosteric effects on the RNase. To this end, several previously characterized type II inhibitors were screened for their ability to block the RNase activity of a recombinant soluble human IRE1 $\alpha$  mini-protein construct containing the kinase/RNase domains—called IRE1 $\alpha$ \* (Supplementary Results, Supplementary Figs. 1 and 2). Since IRE1 $\alpha$ \* is basally autophosphorylated, its RNase is autoactive, and can be assayed using a FRET-quenched XBP1 RNA mini-substrate<sup>7</sup> (Fig. 1b). While all the compounds we tested with this assay contain the core binding elements predicted to stabilize the DFG-out conformation, only one ligand, **1**, demonstrated measurable inhibition of IRE1 $\alpha$ \*'s RNase activity (Fig. 1c,d). **1** is a pyrazolopyrimidine-based inhibitor that has been shown to stabilize the DFG-out conformation of the non-receptor tyrosine kinases Src and Abl. Based on the co-crystal structure of **1** bound to Src (PDB: 3EL8)<sup>24</sup>, proposed contacts with IRE1 $\alpha$  are shown in Fig. 1a.

Despite its modest activity, **1** served as a promising starting point to develop more potent allosteric RNase inhibitors. A number of similar analogs were generated and tested for RNase inhibition. While most modifications of **1** were deleterious, replacing the pyrazolopyrimidine scaffold with an imidazopyrazine core provided a significant increase in overall potency (compound **2**, Fig. 1c,d). Furthermore, substituting the 4-anilino group at the C-3 position of **2** with a naphthylamine moiety provided **3**, the most potent compound

identified in this study. Notably, **3** inhibits XBP1 RNA cleavage to a similar degree as STF-083010, an imine-based small molecule that directly inhibits the IRE1 $\alpha$  RNase through covalent modification<sup>25</sup>.

Similar to APY29, **3** demonstrates dose-dependent reduction of IRE1 $\alpha$ \* kinase autophosphorylation *in vitro* (Fig. 2a and Supplementary Fig. 4). Thus, although **3** and APY29 are both IRE1 $\alpha$ \* kinase inhibitors, they demonstrate opposing effects on its RNase activity, with APY29 acting as a slight activator. To further characterize the differences between the two kinase inhibitors, we generated a version of IRE1 $\alpha$ \* with low basal RNase activity by using  $\lambda$ -phosphatase ( $\lambda$ -PPase) to remove activating phosphates from the enzyme (Fig. 2b and Supplementary Fig. 5). As expected, the dephosphorylated variant of IRE1 $\alpha$ \* (dP-IRE1 $\alpha$ \*) has significantly lower basal RNase activity than IRE1 $\alpha$ \*; incubating dP-IRE1 $\alpha$ \* with increasing APY29 concentrations progressively restores its ability to cleave the XBP1 mini-substrate, plateauing at ~60% of the levels of IRE1 $\alpha$ \* (Figs. 2c,d and Supplementary Fig. 6). In contrast, **3** suppresses the residual RNase activity of dP-IRE1 $\alpha$ \*.

Competition experiments were performed to further explore the opposing effects of APY29 and **3**. Increasing concentrations of APY29 progressively reverse IRE1 $\alpha$ \* RNase inhibition caused by a fixed concentration of **3** (Fig. 2e). On the other hand, increasing concentrations of **3** restore RNase inhibition in the setting of a fixed concentration of APY29, with an expected increase in the IC<sub>50</sub> (Fig. 2e and Supplementary Fig. 7). As predicted, APY29 cannot rescue direct inhibition caused by the covalent RNase modifier STF-083010. Taken together, these results strongly suggest that APY29 and **3** are exerting their opposing effects on RNase activity through the same binding site.

The drug sunitinib is a promiscuous type I inhibitor that has been shown to inhibit the kinase activity of yeast and human IRE1 $\alpha$ <sup>16,19</sup>. To investigate the differences between **3** and other ATP-competitive inhibitors of IRE1 $\alpha$ , we further characterized the interaction of sunitinib with our IRE1 $\alpha$ \* and dP-IRE1 $\alpha$ \* constructs. As expected, sunitinib is a dose-dependent inhibitor of the autophosphorylation activity of IRE1 $\alpha$ \* (Supplementary Fig. 8a). In addition, sunitinib activates the RNase activity of dP-IRE1 $\alpha$ \*, which is consistent with its type I pharmacophore (Supplementary Fig. 8b). Therefore, both APY29 and sunitinib stabilize an ATP-binding site conformation that activates the RNase domain of IRE1 $\alpha$ . Like APY29, increasing amounts of sunitinib are able to rescue the RNase activity of IRE1 $\alpha$ \* in the presence of a fixed concentration of **3** (Supplementary Fig. 8c). Together, these results show that **3** opposes the stereotypic RNase activation demonstrated by various type I ATP-competitive inhibitors of IRE1 $\alpha$ .

### Analysis of the **3**-IRE1 $\alpha$ and APY29-IRE1 $\alpha$ interactions

To further confirm that APY29 and **3** are exerting their opposing effects through the same ATP-binding site, we next turned to a series of biochemical footprinting experiments<sup>26,27</sup>. Specifically, the accessibility of three native cysteine residues within human IRE1 $\alpha$  (Cys572, Cys645, and Cys715) to alkylating agents in the presence or absence of APY29 and **3** was determined (Supplementary Fig. 9). For these studies, electrophilic isotope-coded affinity tag (ICAT) reagents were used to allow a ratiometric and, therefore, quantitative

comparison of alkylation rates<sup>27</sup>. As Cys645 and Cys715 are located within the ATP-binding cleft of IRE1 $\alpha$ , the accessibility of these residues would be expected to be affected by ligands that occupy this site, while Cys572 is a solvent-exposed residue located on the top of the *N*-terminal lobe of the kinase. Consistent with both APY29 and **3** occupying the ATP-binding site of IRE1 $\alpha$ , Cys645, which is located in the kinase hinge region, is highly shielded from alkylating agents in the presence of either inhibitor (Fig. 3a). In contrast, these inhibitors exert opposing effects on the accessibility of Cys715, with APY29 slowing the rate of alkylation and **3** increasing it. Cys715 is located in the activation loop of IRE1 $\alpha$  (two residues C-terminal to the DFG-motif) and the divergent influence of APY29 and **3** on this residue is concordant with these ligands stabilizing different conformations of the activation loop (Fig. 3b). As expected, no detectable difference in the accessibility of Cys572, which is distal to the kinase active site of IRE1 $\alpha$ , is observed in the presence of either inhibitor (Fig. 3c).

Next, we performed molecular docking experiments to obtain a better understanding of how **3** and APY29 interact with the ATP-binding site of human IRE1 $\alpha$ . A model of the DFG-in ATP-binding site conformation was generated from a co-crystal structure of human IRE1 $\alpha$  bound to ADP (PDB code 3P23, chain A)<sup>19</sup>. As a structure of IRE1 $\alpha$  in the DFG-out conformation has not yet been described, a homology model of this conformation was generated by using the activation loop of another kinase—the tyrosine kinase Abl2—as a template. Both the DFG-in and DFG-out models were optimized using multi-step all-atom minimization and explicit water molecular dynamics (MD) simulations<sup>28</sup>. Predictably, the docked structure of APY29 bound to the DFG-in conformation of human IRE1 $\alpha$  is similar to that of this ligand bound to the yeast IRE1 enzyme (Supplementary Fig. 10)<sup>16</sup>. The pyrazole ring of APY29 forms hydrogen bonds with the kinase hinge region and the pyrimidine moiety occupies the adenine pocket. Attempts to obtain a favorable pose of APY29 bound to the DFG-out conformation of IRE1 $\alpha$  were unsuccessful, which is consistent with the ability of this ligand to exclusively stabilize the active conformation of the ATP-binding site.

The most favorable docking pose for **3** bound to the DFG-out conformation of IRE1 $\alpha$  is shown in Figure 3d. In this pose, the imidazopyrazine ring of this ligand forms two hydrogen bonds with the hinge region and occupies the adenine pocket. The bulky naphthyl ring of **3** adopts an almost orthogonal conformation relative to the core scaffold and stacks against the Ile gatekeeper residue. Like other type II inhibitors, the trifluoromethylphenyl moiety of **3** occupies the hydrophobic pocket created by movement of the Phe sidechain in the DFG-motif. While **3** is well accommodated in the DFG-out conformation of human IRE1 $\alpha$ , no favorable poses were observed for this inhibitor bound to the DFG-in conformation. Indeed, our docking studies predict that the only way that **3** can bind to IRE1 $\alpha$  without movement of the DFG motif in the activation loop is if the inhibitor disrupts canonical interactions with the hinge region of the kinase.

To further experimentally test our docking model, we generated analogs of **3** that contain structural elements predicted to lower inhibitor potency (compounds **4** and **5**, Fig. 1d). **4** contains an *N*-methyl group that would be predicted to disrupt its interaction with the hinge region of IRE1 $\alpha$ , and the amide linkage of **5** should not allow the trifluoromethylphenyl

moiety to form as favorable interactions with the hydrophobic pocket created by movement of the DFG-motif. Consistent with our model, both **4** and **5** show a markedly diminished ability to inhibit the RNase activity of IRE1 $\alpha$  compared to **3** (Supplementary Fig. 11).

### **3 and APY29 divergently affect IRE1 $\alpha$ oligomerization**

Self-association of kinase/RNase monomers has been reported to increase RNase activity as dimers and/or higher-order oligomers form in yeast and mammalian IRE1 proteins<sup>11,16,19</sup>. Although it has not been resolved whether IRE1 $\alpha$  RNase activation requires kinase dimerization or high-order oligomerization per se, it is generally accepted that monomeric species are inactive; furthermore, the degree of order may correlate directly with activity<sup>16</sup>. Thus we used APY29 and **3** to test the prediction that they would divergently affect the oligomerization state of human IRE1 $\alpha$  as a basis for their opposing effects on its RNase activity. Specifically, we predicted that RNase activators should drive monomers into higher-order species (dimers and perhaps oligomers) from baseline. To test this prediction, increasing concentrations of IRE1 $\alpha$ \* were incubated with either DMSO, or saturating concentrations of APY29 or **3** and the ratio of oligomeric—defined as all species greater than monomers (mostly dimers)—to monomeric IRE1 $\alpha$  was determined (Fig. 4a). In the absence of ligands, IRE1 $\alpha$ \* shows a concentration-dependent increase in the oligomer/monomer ratio. The presence of APY29 further enhances—whereas **3** decreases—this concentration-dependent increase in the IRE1 $\alpha$ \* oligomer/monomer ratio. Taken together, our *in vitro* data support a model in which these two classes of kinase inhibitors divergently modulate IRE1 $\alpha$ \* RNase activity by exerting opposing effects on the oligomerization state of the enzyme (Fig. 4b).

### **IRE1 $\alpha$ mutants show increased sensitivity to **3****

Having used a truncated form of IRE1 $\alpha$  for all our *in vitro* studies, we next turned to cell-based experiments to test whether we could replicate divergent modulation of the full-length IRE1 $\alpha$  transmembrane protein with the two classes of kinase inhibitors. We first tested and confirmed the on-target effects of **3** using IRE1 $\alpha$  chemical-genetic systems we had previously developed<sup>7</sup>. Specifically, we employed tetracycline-inducible isogenic T-REx 293 stable cell lines expressing either WT or a “holed” IRE1 $\alpha$  gatekeeper mutant<sup>I642A</sup> to determine whether **3** is able to block the RNase activity of IRE1 $\alpha$  *in vivo*. Induced with doxycycline (Dox), the transgenic WT-IRE1 $\alpha$  or IRE1 $\alpha$ <sup>I642A</sup> spontaneously cluster in the ER, *trans*-autophosphorylate and splice XBP1 mRNA, without requiring upstream ER stress (Fig. 5a and Supplementary Figs. 12 and 13). As expected, **3** inhibits autophosphorylation and XBP1 mRNA splicing in the WT cell lines (Supplementary Fig. 13a,b). Consistent with these inhibitory effects occurring through a direct interaction with IRE1 $\alpha$ , control compound **4** does not affect either of these parameters, even at the highest concentration tested (Supplemental Fig. 13c). Furthermore, we hypothesized that the enlarged ATP-binding pocket of IRE1 $\alpha$ <sup>I642A</sup> would better accommodate the bulky C-3 substituent of **3**, leading to enhanced sensitivity. Indeed, our docking studies suggest that the naphthyl ring of **3** is able to occupy a hydrophobic pocket that is accessible in IRE1 $\alpha$ <sup>I642A</sup> and not the wild type protein (Supplementary Fig. 14). Confirming this notion, low nanomolar concentrations of **3** are sufficient to completely block autophosphorylation and XBP1 splicing through this



mutant (Fig. 5a,b and Supplemental Figs. 15 and 16). Furthermore, increasing concentrations of the type I “bumped” inhibitor 1NM-PP1, which is selective for mutant kinases that contain Ala or Gly gatekeeper residues, is able to rescue the RNase activity of IRE1 $\alpha$ <sup>I642A</sup> in the presence of **3** (Fig. 5c and Supplemental Fig. 17).

Our data suggest a model for IRE1 $\alpha$ <sup>I642A</sup>, which can be activated merely through overexpression to basally splice ~50% of cellular XBP1 mRNA, that 1NM-PP1 further increases—while **3** reduces—the activity of the RNase (Supplemental Fig. 18). We propose that these divergent effects proceed from the stabilization of the kinase active site in two distinct modes by these inhibitors, with 1NM-PP1 acting on the “holed” IRE1 $\alpha$ <sup>I642A</sup> kinase in a similar fashion as APY29 does for WT IRE1 $\alpha$ . In summary, the type II pharmacophore **3** likely enforces an inactive kinase conformation in IRE1 $\alpha$ <sup>I642A</sup>, and as it does with WT IRE1 $\alpha$ . Furthermore, **3** may stabilize monomeric IRE1 $\alpha$ <sup>I642A</sup>, while 1NM-PP1 may promote oligomerization, as APY29 does for the WT IRE1 $\alpha$  (Fig. 4b).

### **3 blocks both enzymatic activities of IRE1 $\alpha$ *in vivo***

To further explore how IRE1 $\alpha$  modulators affect the kinase and RNase activities of endogenous IRE1 $\alpha$  under ER stress, we next turned to *in vivo* studies using INS-1 rat insulinoma cell lines, which are derived from insulin-producing pancreatic  $\beta$ -cell tumors and contain large well-developed ERs. These cells were treated with the ER SERCA ATPase pump inhibitor, thapsigargin (Tg), to induce ER stress and IRE1 $\alpha$  activation at levels causing ~50% splicing of cellular XBP1 mRNA (Fig. 6a and Supplemental Fig. 19). Recapitulating our *in vitro* results, **3** and APY29 demonstrate opposing dose-dependent effects on ER stress-induced activation of the RNase of endogenous IRE1 $\alpha$  (Fig. 6a and Supplemental Fig. 19). Furthermore, **3** abrogates IRE1 $\alpha$  autophosphorylation at a similar concentration as it blocks RNase activity (Fig. 6b,c and Supplemental Figs. 20 and 21). Control compound **4** does not block the splicing of XBP1 mRNA (Fig. 6d and Supplemental Fig. 22). Consistent with its *in vitro* activity, the type I inhibitor sunitinib is able to partially inhibit the kinase activity of IRE1 $\alpha$ , but has no effect on the RNase activity of this enzyme (Fig. 6b,c and Supplemental Figs. 20 and 21) at the concentrations tested. The RNase inhibitor STF-083010 was also tested in INS-1 cells that had been treated with Tg. As expected, this compound inhibits XBP1 splicing in a dose-dependent manner, but does not prevent IRE1 $\alpha$  auto-phosphorylation (Fig. 6b,c and Supplemental Figs. 20 and 21). Therefore, **3** is the only compound identified to date that has the ability to block both enzymatic activities of IRE1 $\alpha$ , both *in vitro* and *in vivo* (Fig. 6e).

## **Discussion**

Recent studies show that the duration and amplitude of UPR activation powerfully affects both cell function and fate<sup>7,8,29,30</sup>. Indeed, many cell-degenerative diseases such as diabetes mellitus feature increased ER stress and UPR activation in affected cells<sup>3,31,32</sup>. These same markers are evident in a wide range of solid and hematopoietic malignancies<sup>33</sup>. To properly ascertain the role of the UPR in these disease contexts will require development of tool compounds that target critical nodes in the UPR in both positive and negative directions. The master UPR regulator IRE1 $\alpha$ , which controls cell fate under ER stress, offers two

enzymatic targets that could be modulated with small molecules. In this work, we exploited the unusual mechanistic relationship between these two catalytic domains to inhibit the RNase from a distance by inhibiting the kinase.

Starting with known pharmacophores that stabilize an inactive conformation in other protein kinases, we optimized a type II inhibitor lead to produce **3**. Despite inhibiting IRE1 $\alpha$  kinase autophosphorylation similarly to the type I inhibitor APY29, **3** inhibits XBP1 mRNA splicing, even during ER stress. Consistent with competition studies, footprinting experiments strongly suggest that **3** and APY29 bind to the same ATP-binding pocket. However, these same footprinting experiments indicate that these inhibitors cause divergent effects on the activation loop of IRE1 $\alpha$ , and support a model in which **3** and APY29 promote distinct, mutually exclusive, movements of the DFG-motif contained within the activation loop.

The aforementioned experiments, combined with modeling studies, lead to a parsimonious model of IRE1 $\alpha$  modulation by kinase inhibitors (Fig. 6e) that posits that the protein can adopt either a canonical DFG-in or a DFG-out conformation, as is seen with other kinases under the influence of types I and II inhibitors, respectively. However, while for other kinases these two distinct modes of inhibition stereotypically shut down kinase function, for the multi-domain kinase, IRE1 $\alpha$ , the two inhibition modes have opposite and divergent results on the attached RNase activity. To our knowledge, this ability to modulate a second catalytic activity in a multi-domain kinase in two different directions with distinct classes of ATP-competitive inhibitors has not been reported to date. We expect that this ability may be extended to many of the other known multi-domain kinases.

Intriguingly, opposite effects on oligomeric state were found using the two compounds: while type I inhibitors increase the dimeric and possibly oligomeric state of IRE1 $\alpha$  and the catalytic activity of the RNase, type II inhibitors decrease both in tandem. Given previous reports of a direct mechanistic relationship between the degree of order and RNase activity in IRE1 proteins<sup>16</sup>, we speculate that the inactive conformation that **3** stabilizes in IRE1 $\alpha$  promotes the monomeric state.

It is of course conceivable that a different, previously unidentified active site conformation is adopted in the presence of **3**; to fully resolve this particular point in the future will require atomic level co-crystal structures. Regardless, the particular kinase active site conformation stabilized by **3** has the unique and novel property of preserving the mechanistic coupling between the kinase and the RNase in IRE1 $\alpha$ , allowing full inhibition of both activities in concert. We propose that this represents a new alternative to aldehyde-based covalent inhibitors of the RNase such as STF-083010 (or another recently reported compound called 4 $\mu$ 8C<sup>34</sup>), which leave kinase autophosphorylation and oligomerization intact. In contrast to the action of direct RNase inhibitors, any biological signaling through the kinase that is dependent on phosphorylation of non-autonomous substrates or kinase-mediated scaffolding should be simultaneously quenched with type II kinase inhibitors.

In summary, the ability to now inhibit the effector RNase domain of IRE1 $\alpha$  with type II kinase inhibitors complements our previous ability to activate the RNase with type I



inhibitors, independent of upstream ER stress, establishing opposite directions of control over this master UPR regulator. Thus, type II kinase inhibitors of IRE1 $\alpha$  will expand on a toolkit that includes chemical-genetic systems to test and validate the UPR's role in ER stress-related diseases. While **3** is not completely selective for IRE1 $\alpha$  over other protein kinases, this compound serves as a starting point for the generation of more potent and selective inhibitors that may eventually be developed into disease-modifying drugs for ER stress-related disorders. Moreover, the ability to toggle the IRE1 $\alpha$  RNase on and off through its kinase domain may serve as a precedent for pharmacologically targeting the many other kinase-coupled enzymes present in eukaryotes.

## Methods

Synthesis and characterization of probes are described in the Supplementary Methods.

### Expression and purification of IRE1 $\alpha$ \* and dP-IRE1 $\alpha$ \*

A construct containing the cytosolic kinase and RNase domains of human IRE1 $\alpha$  (residues 469–977, IRE1 $\alpha$ \*) was expressed in SF9 insect cells by using Bac-to-Bac baculovirus expression system (Invitrogen) with a 6-His-tag at the N-terminus, and purified with a Ni-NTA (Qiagen) column. To generate dP-IRE1 $\alpha$ \*, basal phosphorylation sites were removed by incubating IRE1 $\alpha$ \* with  $\lambda$ -PPase (NEB) at a molar ratio of 5:1 (IRE1 $\alpha$ \*:  $\lambda$ -PPase) in 50 mM HEPES pH 7.5, 100 mM NaCl, 1 mM MnCl<sub>2</sub>, 2 mM DTT, 0.01% Brij 35 for 40 min at RT. Dephosphorylation was verified by immunoblotting with an anti-phosphoIRE1 $\alpha$  antibody.

### Kinase assays

Inhibitors (initial concentration = 80  $\mu$ M, 2-fold serial dilutions) were incubated with IRE1 $\alpha$ \* in cleavage buffer (20 mM Hepes at pH 7.5, 0.05% Triton X100, 50mM KOAC, 1 mM Mg(OAC)<sub>2</sub>, 1 mM DTT) for 20 min, followed by incubation with 10  $\mu$ Ci [ $\gamma$ -<sup>32</sup>P]ATP (3000 Ci/mmol, Perkin Elmer) at RT for 30 min. Samples were then separated by SDS-PAGE, and autoradiographed. The auto-phosphorylation level were quantified by setting the band intensity of IRE1 $\alpha$ \* without compound treatment as 1 and the background as 0.

### In vitro RNase assay

5'FAM-3'BHQ-labeled XBP1 single stem-loop minisubstrate (5'FAM-CUGAGUCCGACACUCAG-3'BHQ) was purchased from Dharmacon. 0.2  $\mu$ M IRE1 $\alpha$ \* or dP-IRE1 $\alpha$ \* were incubated with inhibitors or DMSO for 20 min in cleavage buffer, followed by incubation with 3  $\mu$ M RNA substrate for 5 min. The reaction was quenched by adding urea to a final concentration of 4 M, and the fluorescence was detected on a SpectraMax M5 microplate reader (Molecular Devices) with excitation and emission wavelengths of 494 nm and 525 nm, respectively. The fluorescence intensities were normalized by setting the signal for the reaction with IRE1 $\alpha$ \* and DMSO to 1 and the reaction without IRE1 $\alpha$ \* to 0. The cleavage products were also resolved by urea PAGE after phenol/chloroform extraction and ethanol precipitation. Internally <sup>32</sup>P-labelled mouse XBP1 RNA was also used as a substrate, as described<sup>7</sup>.

## ICAT Footprinting

Heavy and light iodinated ICAT reagents were made as described by Underbakke et al<sup>27</sup>. Purified human Ire1 $\alpha$  was exchanged into 50 mM Tris (pH 8.0), 50 mM KCl, 5 mM MgCl<sub>2</sub>, and 0.5 mM TCEP. One 3  $\mu$ M stock solution was divided into three solutions, and each was mixed with either DMSO, APY29, or **5** to yield solutions containing 1% DMSO and 20  $\mu$ M of inhibitor. Heavy labeling reagent was added to the protein solutions, and 25  $\mu$ L aliquots were taken at specified times and quenched with excess DTT. Samples were precipitated with 0.2% sodium deoxycholate and 10% trichloroacetic acid on ice for 10 min. The mixtures were centrifuged at 4 °C for 15 min, and pellets were washed with cold acetone. The pellets were then resuspended in 30  $\mu$ L of 200 mM Tris (pH 8.0), 7 M urea, and 2.4 mM light labeling reagent, and incubated in the dark for 30 min. The solutions were diluted with 210  $\mu$ L 200 mM Tris (pH 8.0), 5.7 mM CaCl<sub>2</sub>, 0.5  $\mu$ g porcine trypsin (TPCK treated, Sigma), and 125 ng GluC (Roche), and incubated at room temperature overnight. Samples (0.3 pmol) were injected onto a Thermo Scientific Dionex Acclaim Pepmap100 NanoLC capillary column (C<sub>18</sub>, 150 mm length, I.D. 75  $\mu$ m, 3  $\mu$ m particle size) connected inline to a Finnigan LCQ mass spectrometer. Peptides of interest were identified by MS/MS data (Sequest), and corresponding XIC peaks were integrated. Alkylation curves were fit using GraphPad Prism software (Binding – Kinetics, Dissociation – One-phase exponential decay).

## IRE1 $\alpha$ \* Cross-linking to determine oligomer to monomer ratio

Increasing concentrations of IRE1 $\alpha$ \* (0.49–30  $\mu$ M) were incubated with DMSO, **3** (200  $\mu$ M), or APY29 (200  $\mu$ M) for 20 min, then cross-linked by adding 250  $\mu$ M disuccinimidyl suberate (DSS) (Pierce) for 1 hr at RT in cleavage buffer. The reaction was quenched by addition of 50 mM Tris-HCl (pH 7.5). The samples were then boiled, resolved on SDS-PAGE, and immunoblotted for IRE1 $\alpha$  with an anti-IRE1 $\alpha$  antibody, (visualization and quantification with a LI-COR Odyssey scanner).

## Cell culture and XBP1 mRNA splicing

INS-1 cells were grown in RPMI, 10% fetal calf serum, 1 mM sodium pyruvate, 10 mM HEPES, Pen/strep, 2 mM glutamine and 50  $\mu$ M  $\beta$ -mercaptoethanol. T-Rex 293 IRE1 $\alpha$  or IRE1 $\alpha$ <sup>I642A</sup> were grown in DME H-21 with 10% fetal calf serum and Pen/strep. After 1 hr incubation with compounds, INS-1 cells were treated with 6 nM thapsigargin for 4 hrs, and T-Rex 293 IRE1 $\alpha$ -expressing cells were treated with 1  $\mu$ M Dox for 8 hrs. The RNA was then extracted using RNeasy Mini Kit (Qiagen), and reverse transcribed using the QuantiTect Reverse Transcription Kit (Qiagen). XBP1 splicing was performed as previously described<sup>7</sup>. Primers used: sense primer rXBP 1.3S (5'-AAACAGAGTAGCAGCACAGACTGC-3'') and antisense primer rXBP 1.2AS (5'-GGATCTCTAAGACTAGAGGCTTGGTG-3') for INS-1 cell line, while sense primer mXBP1.3S (5'-AAACAGAGTAGCAGCGCAGACTGC-3') and antisense primer mXBP1.2AS (5'-GGATCTCTAAAAGACTAGAGGCTTGGTG-3') for T-Rex 293 cell line. PCR products were resolved on 2.5% agarose gels, stained with EtBr, and quantified by ImageJ.

## Statistical analysis

All experiments were performed in triplicate, unless otherwise specified. Results are shown as mean  $\pm$  standard deviation (SD).

## Other methods

Detailed information is available in the Supplementary Methods.

## Supplementary Material

Refer to Web version on PubMed Central for supplementary material.

## Acknowledgements

This work was supported by NIH: Director's New Innovator Award DP2 OD001925 (F.R.P), RO1 DK080955 (F.R.P), RO1 CA136577 (S.A.O.), RO1 GM086858 (D.J.M); an American Cancer Society Research Scholar Award (S.A.O.) and the Burroughs Wellcome (F.R.P.) and Sloan (D.J.M) Foundations. S.B.H was supported by a predoctoral fellowship from the American Heart Association.

## References

1. Walter P, Ron D. The unfolded protein response: from stress pathway to homeostatic regulation. *Science*. 2011; 334:1081–1086. [PubMed: 22116877]
2. Merksamer PI, Papa FR. The UPR and cell fate at a glance. *J. Cell. Sci.* 2010; 123:1003–1006. [PubMed: 20332117]
3. Scheuner D, Kaufman RJ. The unfolded protein response: a pathway that links insulin demand with beta-cell failure and diabetes. *Endocr. Rev.* 2008; 29:317–333. [PubMed: 18436705]
4. Carrasco DR, et al. The differentiation and stress response factor XBP-1 drives multiple myeloma pathogenesis. *Cancer Cell*. 2007; 11:349–360. [PubMed: 17418411]
5. Tabas I, Ron D. Integrating the mechanisms of apoptosis induced by endoplasmic reticulum stress. *Nat. Cell. Biol.* 2011; 13:184–190. [PubMed: 21364565]
6. Tirasophon W, Welihinda AA, Kaufman RJ. A stress response pathway from the endoplasmic reticulum to the nucleus requires a novel bifunctional protein kinase/endoribonuclease (Ire1p) in mammalian cells. *Genes Dev.* 1998; 12:1812–1824. [PubMed: 9637683]
7. Han D, et al. IRE1alpha kinase activation modes control alternate endoribonuclease outputs to determine divergent cell fates. *Cell*. 2009; 138:562–575. [PubMed: 19665977]
8. Han D, et al. A kinase inhibitor activates the IRE1alpha RNase to confer cytoprotection against ER stress. *Biochem. Biophys. Res. Commun.* 2008; 365:777–783. [PubMed: 18035051]
9. Lin J, et al. IRE1 Signaling Affects Cell Fate During the Unfolded Protein Response. *Science*. 2007; 318:944–949. [PubMed: 17991856]
10. Credle JJ, Finer-Moore JS, Papa FR, Stroud RM, Walter P. On the mechanism of sensing unfolded protein in the endoplasmic reticulum. *Proc. Natl. Acad. Sci. USA*. 2005; 102:18773–18784. [PubMed: 16365312]
11. Zhou J, et al. The crystal structure of human IRE1 luminal domain reveals a conserved dimerization interface required for activation of the unfolded protein response. *Proc. Natl. Acad. Sci. USA*. 2006; 103:14343–14348. [PubMed: 16973740]
12. Gardner BM, Walter P. Unfolded proteins are Ire1-activating ligands that directly induce the unfolded protein response. *Science*. 2011; 333:1891–1894. [PubMed: 21852455]
13. Calton M, et al. IRE1 couples endoplasmic reticulum load to secretory capacity by processing the XBP-1 mRNA. *Nature*. 2002; 415:92–96. [PubMed: 11780124]
14. Yoshida H, Matsui T, Yamamoto A, Okada T, Mori K. XBP1 mRNA is induced by ATF6 and spliced by IRE1 in response to ER stress to produce a highly active transcription factor. *Cell*. 2001; 107:881–891. [PubMed: 11779464]

15. Papa FR, Zhang C, Shokat K, Walter P. Bypassing a kinase activity with an ATP-competitive drug. *Science*. 2003; 302:1533–1537. [PubMed: 14564015]
16. Korennykh AV, et al. The unfolded protein response signals through high-order assembly of Ire1. *Nature*. 2009; 457:687–693. [PubMed: 19079236]
17. Liu Y, Gray NS. Rational design of inhibitors that bind to inactive kinase conformations. *Nat. Chem. Biol.* 2006; 2:358–364. [PubMed: 16783341]
18. Korennykh AV, et al. Cofactor-mediated conformational control in the bifunctional kinase/RNase Ire1. *BMC Biol.* 2011; 9:48. [PubMed: 21729334]
19. Ali MM, et al. Structure of the Ire1 autophosphorylation complex and implications for the unfolded protein response. *EMBO J.* 2011; 30:894–905. [PubMed: 21317875]
20. Lee KP, et al. Structure of the dual enzyme Ire1 reveals the basis for catalysis and regulation in nonconventional RNA splicing. *Cell*. 2008; 132:89–100. [PubMed: 18191223]
21. Wan PT, et al. Mechanism of activation of the RAF-ERK signaling pathway by oncogenic mutations of B-RAF. *Cell*. 2004; 116:855–867. [PubMed: 15035987]
22. Schindler T, et al. Structural mechanism for STI-571 inhibition of abelson tyrosine kinase. *Science*. 2000; 289:1938–1942. [PubMed: 10988075]
23. Ranjitkar P, Brock AM, Maly DJ. Affinity reagents that target a specific inactive form of protein kinases. *Chem. Biol.* 2010; 17:195–206. [PubMed: 20189109]
24. Dar AC, Lopez MS, Shokat KM. Small molecule recognition of c-Src via the Imatinib-binding conformation. *Chem. Biol.* 2008; 15:1015–1022. [PubMed: 18940662]
25. Papandreou I, et al. Identification of an Ire1 $\alpha$  endonuclease specific inhibitor with cytotoxic activity against human multiple myeloma. *Blood*. 2011; 117:1311–1314. [PubMed: 21081713]
26. Tu BP, Wang JC. Protein footprinting at cysteines: probing ATP-modulated contacts in cysteine-substitution mutants of yeast DNA topoisomerase II. *Proc. Natl. Acad. Sci. USA*. 1999; 96:4862–4867. [PubMed: 10220384]
27. Underbakke ES, Zhu Y, Kiessling LL. Isotope-coded affinity tags with tunable reactivities for protein footprinting. *Angew. Chem. Int. Ed.* 2008; 47:9677–9680.
28. Bowers, KJ., et al. Proceedings of the ACM/IEEE Conference on Supercomputing (SC06); Tampa, Florida, USA. 2006.
29. Yoshida H, et al. A time-dependent phase shift in the mammalian unfolded protein response. *Dev. Cell*. 2003; 4:265–271. [PubMed: 12586069]
30. Lu PD, et al. Cytoprotection by pre-emptive conditional phosphorylation of translation initiation factor 2. *EMBO J.* 2004; 23:169–179. [PubMed: 14713949]
31. Huang CJ, et al. High Expression Rates of Human Islet Amyloid Polypeptide Induce Endoplasmic Reticulum Stress-Mediated Beta Cell Apoptosis, a Characteristic of Humans with Type 2 but Not Type 1 Diabetes. *Diabetes*. 2007
32. Oyadomari S, et al. Targeted disruption of the Chop gene delays endoplasmic reticulum stress-mediated diabetes. *J. Clin. Invest.* 2002; 109:525–532. [PubMed: 11854325]
33. Feldman DE, Chauhan V, Koong AC. The unfolded protein response: a novel component of the hypoxic stress response in tumors. *Mol Cancer Res*. 2005; 3:597–605. [PubMed: 16317085]
34. Cross BC, et al. The molecular basis for selective inhibition of unconventional mRNA splicing by an IRE1-binding small molecule. *Proc Natl Acad Sci U S A*. 2012; 109:E869–E878. [PubMed: 22315414]
35. Salah E, et al. Crystal structures of ABL-related gene (ABL2) in complex with imatinib, tozasertib (VX-680), and a type I inhibitor of the triazole carbothioamide class. *J. Med. Chem.* 2011; 54:2359–2367. [PubMed: 21417343]

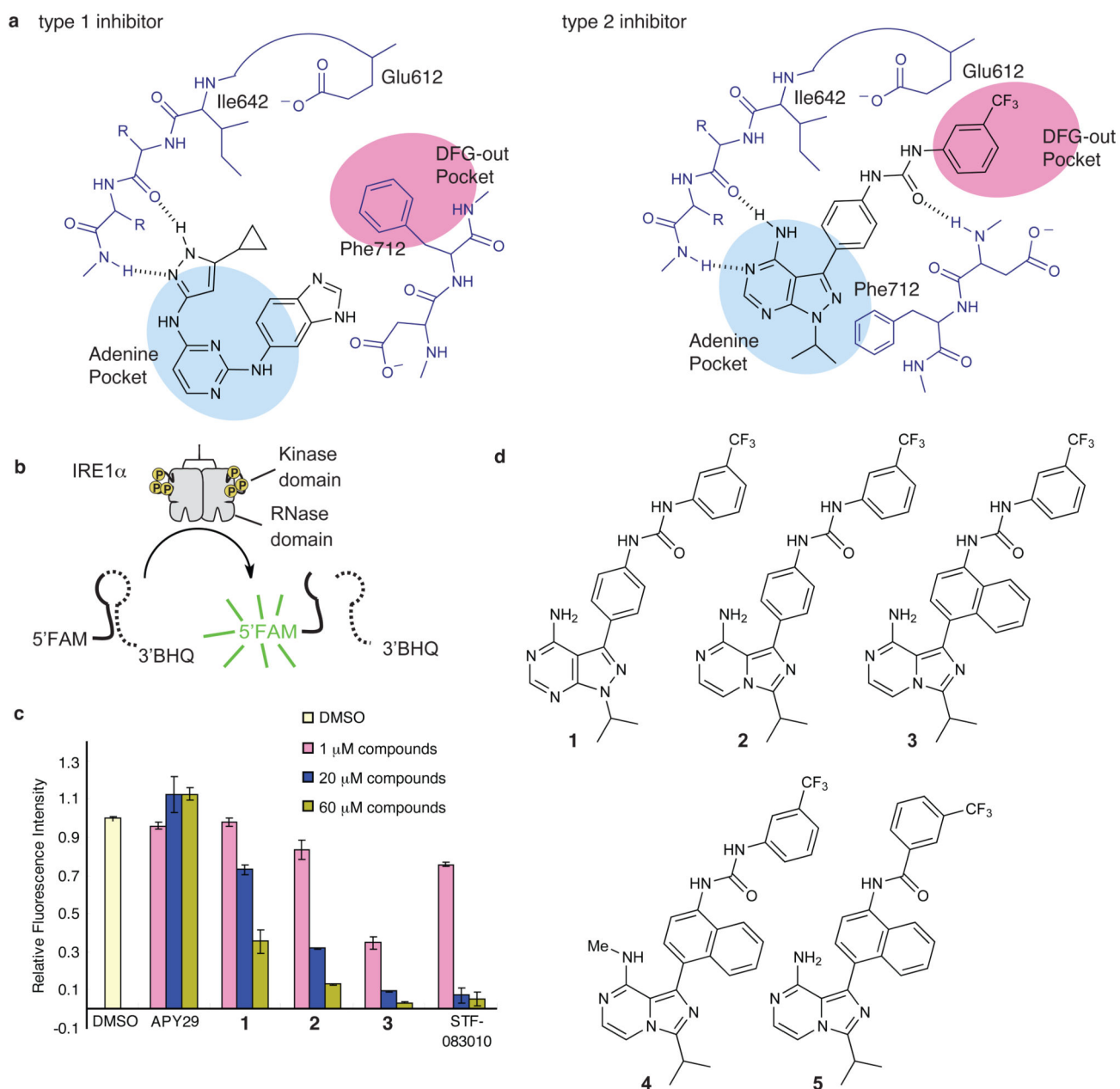


**Figure 1. Interaction of ATP-competitive inhibitors with the bifunctional kinase/RNase, IRE1 $\alpha$**   
**(a)** Proposed binding modes of type I and type II kinase inhibitors with the ATP-binding pocket of IRE1 $\alpha$ . Left panel shows the contacts the type I inhibitor APY29 forms with yeast IRE1 $\alpha$  (PDB code 3SDJ)<sup>18</sup>. The right panel shows the proposed contacts a type II inhibitor **1** forms with IRE1 $\alpha$  based on the co-crystal structure of the same inhibitor bound to Src (PDB code 3EL8) (also see Supplementary Fig. 3). **(b)** XBP1 RNA minisubstrate assay used for screening IRE1 $\alpha$  modulators. The recombinant human IRE1 $\alpha$ —IRE1 $\alpha^*$ —used in the assay spans residues 469–977, which includes the cytosolic kinase and RNase domains. Cleavage of the 5'FAM-3'BHQ-labeled XBP1 minisubstrate by IRE1 $\alpha^*$  results in FRET-dequenching. **(c)** Endpoint fluorescence of IRE1 $\alpha^*$  catalyzed cleavage reaction of XBP1

minisubstrate in the presence of varying concentrations of inhibitors, or DMSO. STF-083010 is an imine-based compound that covalently inhibits the RNase domain. Relative fluorescence intensity is scaled to the signal observed with IRE1 $\alpha^*$  (1.0), or without IRE1 $\alpha^*$  (0). (mean  $\pm$  SD, n = 3). **(d)** Structures of the type II kinase inhibitors used in this study.

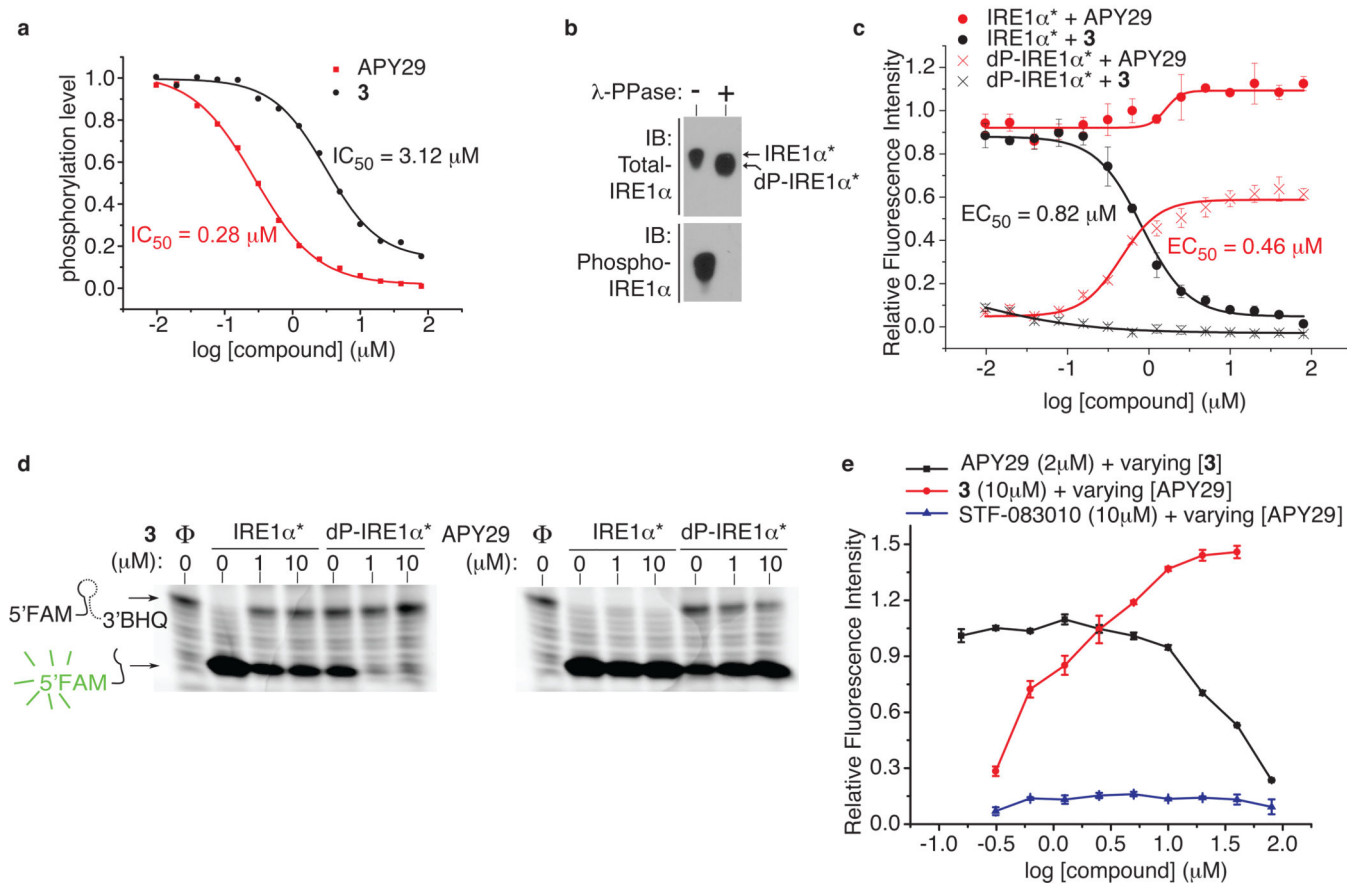
Author Manuscript

Author Manuscript

Author Manuscript

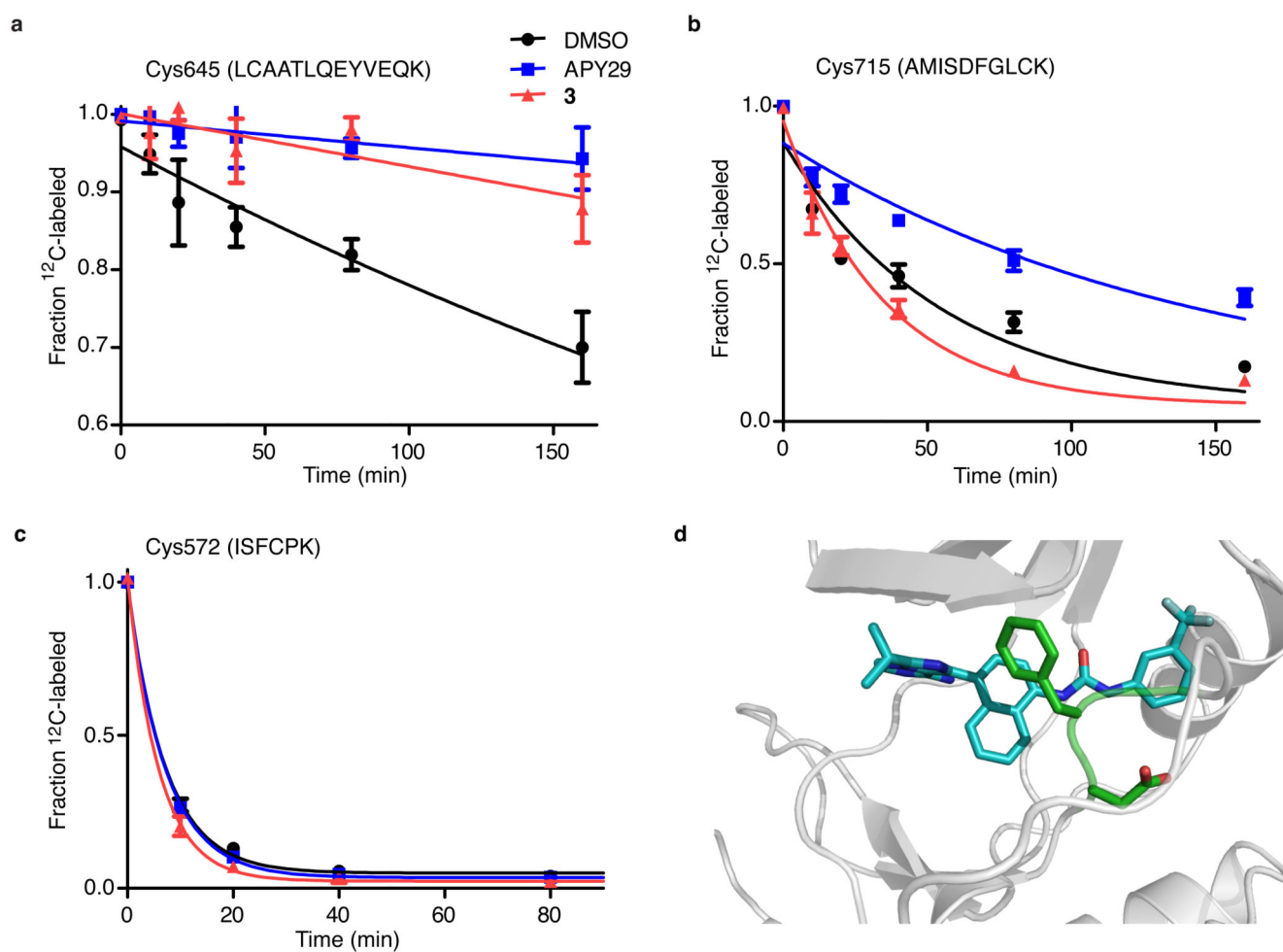
Author Manuscript





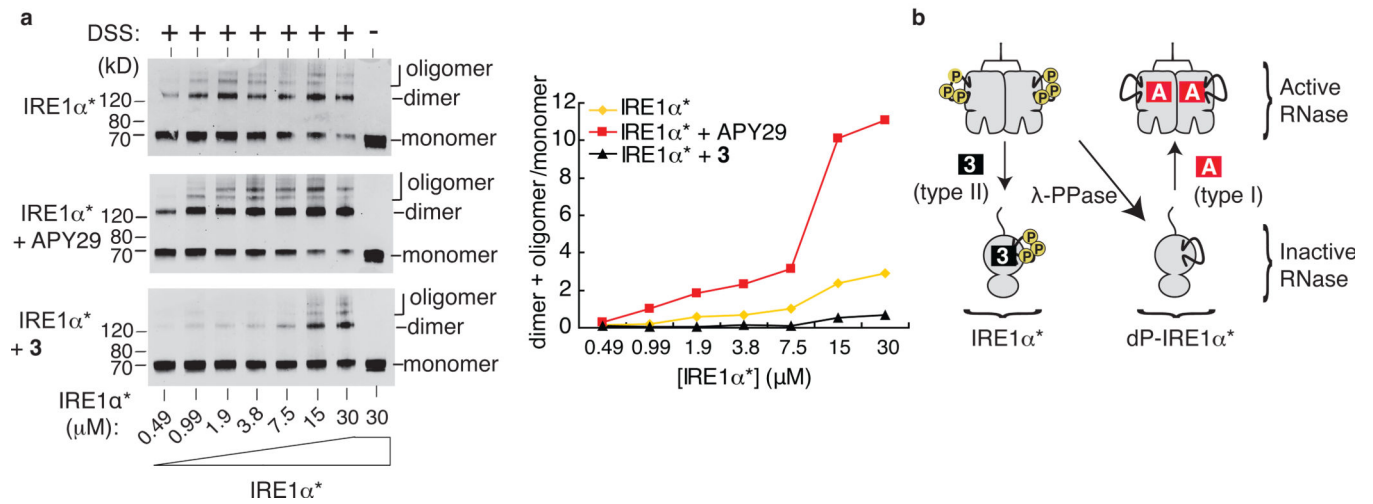
**Figure 2. APY29 and 3 divergently modulate the RNase activity and oligomerization state of IRE1 $\alpha^*$**

(a) Inhibition of IRE1 $\alpha^*$  autophosphorylation *in vitro* by APY29 and 3. Normalized autophosphorylation levels and  $IC_{50}$  values for both compounds are shown. (b)  $\lambda$ -PPase treatment of IRE1 $\alpha^*$  produces dephosphorylated IRE1 $\alpha^*$  (dP-IRE1 $\alpha^*$ ). Immunoblots using anti-IRE1 $\alpha$  and anti-phospho IRE1 $\alpha$  antibodies are shown. (c) RNase activities of IRE1 $\alpha^*$  and dP-IRE1  $\alpha^*$  under varying concentrations of APY29 or 3 per the assay of Figure 1b.  $EC_{50}$  values were determined by fitting normalized fluorescence intensities (mean  $\pm$  SD, n = 3). (d) Urea PAGE of XBP1 mini-substrate cleavage by IRE1 $\alpha^*$  and dP-IRE1 $\alpha^*$  with and without 3 or APY29. (e) RNase competition assays between APY29 and 3. The red line shows IRE1 $\alpha^*$  RNase activity under fixed 3 and varying APY29 concentrations. The black line shows IRE1 $\alpha^*$  RNase activity under fixed APY29 and varying 3 concentrations. The blue line shows IRE1 $\alpha^*$  RNase activity under fixed STF-083010 and varying APY29 concentrations (mean  $\pm$  SD, n = 3).



### Figure 3. Characterization of 3's interaction with the ATP-binding site of IRE1α

Results of the ICAT footprinting experiments with IRE1α\*. Alkylation rates were measured in the presence of DMSO (black), APY29 (blue) (20 μM), or 3 (red) (20 μM) (mean ± SD, n = 3). **(a)** Alkylation rate of Cys572. **(b)** Alkylation rate of Cys645. **(c)** Alkylation rate of Cys715. **(d)** A molecular model of 3's interaction with the ATP-binding site of IRE1α (grey). IRE1α is in the DFG-out inactive conformation. The imidazopyrazine ring of 3 occupies the adenine pocket and the 3-trifluoromethylurea occupies the DFG-out pocket. No favorable poses for 3 bound to the DFG-in conformation of IRE1α could be determined.



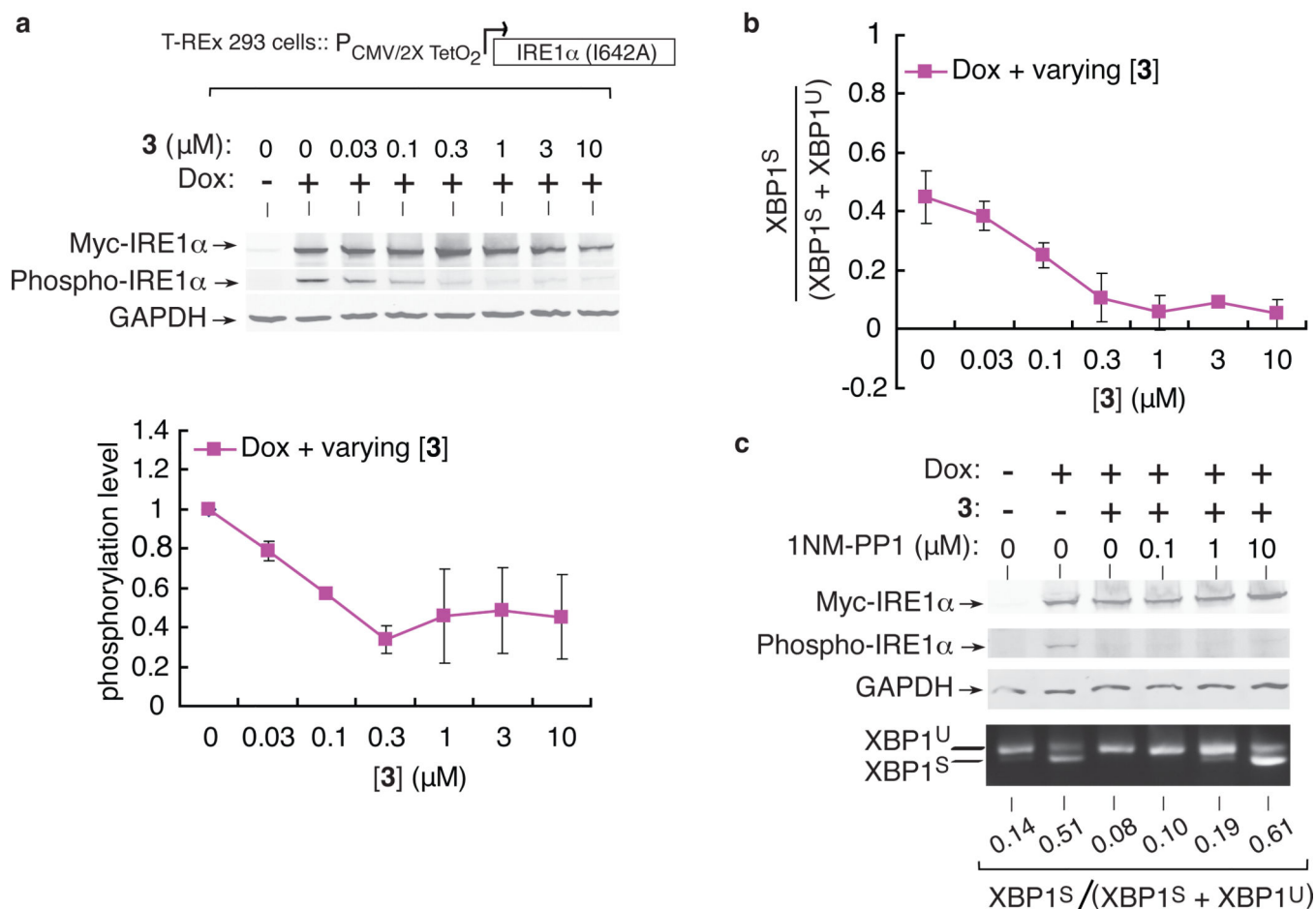


**Figure 5. Chemical-genetic modulation of IRE1 $\alpha$  kinase and RNase activity *in vivo***

(a) Anti-total and anti-phospho IRE1 $\alpha$  immunoblots of T-Rex 293 cells expressing “holed” IRE1 $\alpha$ <sup>I642A</sup> under Doxycycline (Dox) control. Cells were pre-treated for 1 hr with **3** at indicated concentrations, then induced with Dox (1  $\mu$ M) for 8 hrs. Plots show normalized phosphorylation levels and ratios of spliced XBP1 mRNA under varying concentrations **3** (mean  $\pm$  SD, n  $\geq$  3). (b) Quantification of the XBP1 cDNA amplicons from the cells described in (a). EtBr-stained agarose gels are shown in Supplementary Figure 16 (c). Competition between the “bumped” kinase inhibitor 1NM-PP1 and **3** against IRE1 $\alpha$ <sup>I642A</sup>. T-Rex 293 cells expressing IRE1 $\alpha$ <sup>I642A</sup> were pre-treated for 1 hr with **3** (1  $\mu$ M)  $\pm$  varying concentrations 1NM-PP1 before Dox induction (1  $\mu$ M) for 8 hrs. Quantification show ratios of spliced XBP1 mRNA as a function of **3** and 1NM-PP1 concentrations. [XBP1<sup>S</sup> = spliced XBP1; XBP1<sup>U</sup> = unspliced XBP1]

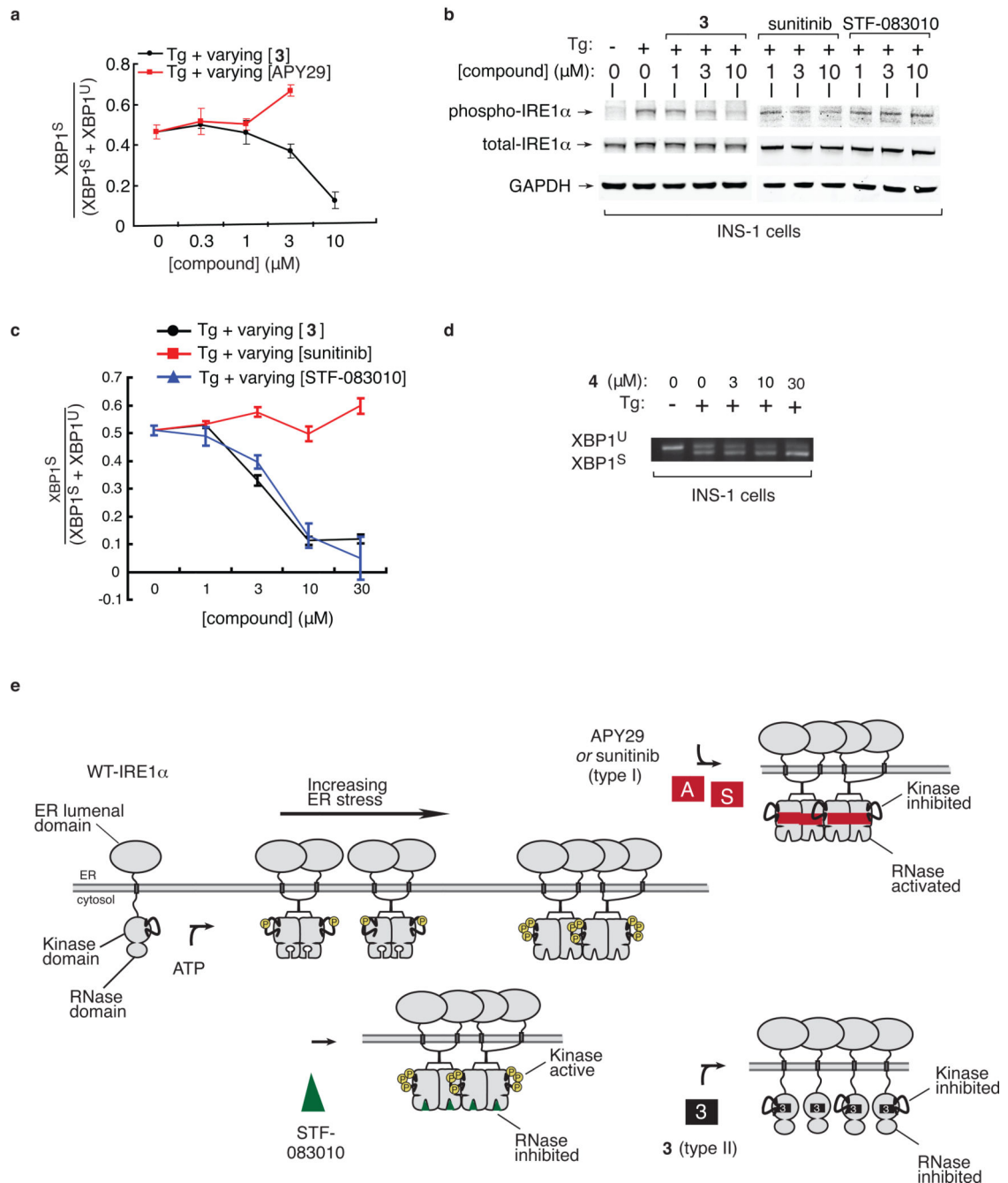


**Figure 6. Divergent modulation of endogenous IRE1α RNase activity under ER stress with types I and II kinase inhibitors**

(a) Quantification of EtBr-stained agarose gel of XBP1 complementary DNA (cDNA) amplicons from INS-1 cells pre-treated for 1 hr with **3** or APY29 at indicated concentrations, followed by Tg (6 nM) for 4 hrs. Ratios of XBP1<sup>S</sup> over (XBP1<sup>S</sup> + XBP1<sup>U</sup>) are plotted (mean ± SD, n = 3). Gels are shown in Supplemental Figure 19. (b) Anti-total and anti-phospho IRE1α immunoblots using extracts from INS-1 cells pre-treated for 1 hr with **3**, sunitinib or STF-083010 at indicated concentrations, followed by Tg (6 nM) for 2

hrs. (c) Quantification of EtBr-stained agarose gel of XBP1 complementary DNA (cDNA) amplicons from the INS-1 cells described in (b). Gels are shown in Supplemental Figure 20. (d) EtBr-stained agarose gel of XBP1 cDNA amplicons from INS-1 cells pre-treated for 1 hr with **4** at indicated concentrations, followed by Tg (6 nM) for 4 hrs. (e) Model of how type I kinase inhibitors (APY29 or sunitinib), type II kinase inhibitors (**3**), and RNase inhibitors (STF-083010) modulate the enzymatic activities of WT IRE1 $\alpha$ . APY29 inhibits IRE1 $\alpha$  *trans*-autophosphorylation but promotes oligomerization and activates the RNase domain. STF-083010 inhibits the RNase activity of IRE1 $\alpha$  but does not affect kinase activity or the overall oligomerization state. **3** inhibits both the kinase and RNase domains of IRE1 $\alpha$  and stabilizes the monomeric form. [Please note that these cartoons are not meant to differentiate between the relative orientations of monomer subunits in IRE1 $\alpha$ .]